ACCOUNTS
of chemical research

Cross-Conjugated Cruciform Fluorophores

ANTHONY J. ZUCCHERO, PSARAS L. MCGRIER, AND
UWE H. F. BUNZ*

School of Chemistry and Biochemistry, Georgia Institute of Technology, 901 Atlantic Drive, Atlanta, Georgia 30332

RECEIVED ON JULY 31, 2009

CONSPECTUS

In optoelectronic devices, chromophores can be designed at the molecular level to create materials with properties desired for advanced applications. Organic fluorophores in particular can be constructed with macroscopic properties that arise from two distinct contributions: (i) the collective impact of the molecular backbone and substituents and (ii) the connectivity within the molecule (that is, the spatial molecular architecture). Accordingly, the exploration of novel conjugated architectures is a productive area of current research.

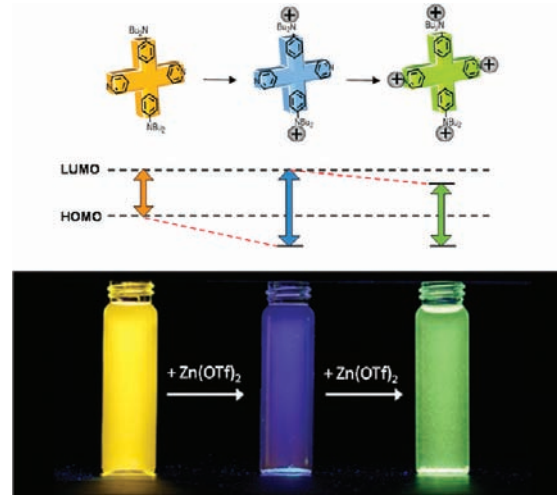

Different two-dimensional, "X-shaped" conjugated materials have been synthesized for a variety of applications. They include spiro compounds, paracyclophanes, swivel-type dimers, bisoxazole-derived cruciforms, tetraethynylethenes, and tetrasubstituted tolanes. A subset of these compounds are constructed from two "perpendicular" π-conjugated linear arms connected through a central aromatic core; examples of these include tetrakis(arylethynyl)benzenes, tetrakis(styryl)benzenes, and tetrasubstituted thiophenes.

In this Account, we evaluate 1,4-distyryl-2,5-bis(arylethynyl)benzenes or cruciforms (XFs). Electronic substitution of this "X-shaped" cross-conjugated scaffold tunes both the energy levels of the frontier molecular orbitals (FMOs) and their spatial distribution in XFs. The resulting fluorophores exhibit FMO separation, imbuing XFs with unusual yet desirable properties for sensory applications.

Using model analytes, we examine how the underlying FMO arrangement and the nature of analyte interaction elicit observable responses. These studies provide a foundation for accessing functional responsive ratiometric cores, demonstrating the importance and unique potential of FMO-separated fluorophores.

We also highlight the essential contribution of serendipity in materials development. Moving beyond one-dimensional molecular wire-type fluorophores to two-dimensional "X-shaped" materials provides access to materials with unexpected and exciting properties. XFs represent such novel conjugated architectures, and their successful development has frequently has hinged on inspiration from structural components and principles developed in diverse research areas.

Introduction

Conjugated organic materials have attracted interest as fluorescent sensors and components in organic electronics. For dyes to exhibit ratiometric sensory responses, the interaction of an analyte must elicit a change in the fluorophore's HOMO−LUMO gap. This necessitates that one frontier molecular orbital (FMO) must be disproportionally affected by analyte interaction. In the majority of organic fluorophores, the HOMO and LUMO are "congruent"; that is, their orbital coefficients are of similar magnitude. One would not expect large shifts in color or emission wavelength upon binding to an analyte; the position

Published on the Web 12/04/2009 www.pubs.acs.org/acr
10.1021/ar900218d

SCHEME 1. Generalized Synthetic Pathway Providing Access to Cruciforms

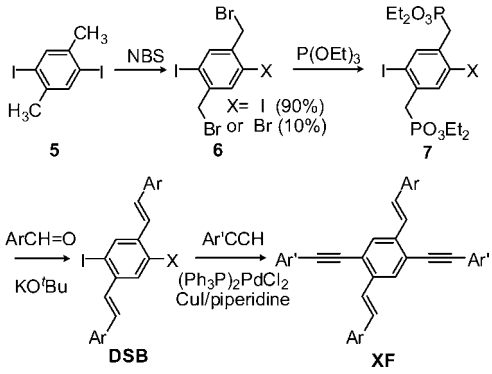

SCHEME 2. Synthesis of Hydroxy-Functionalized Cruciforms **12**−**14** via Sequential Horner and Sonogashira Couplings

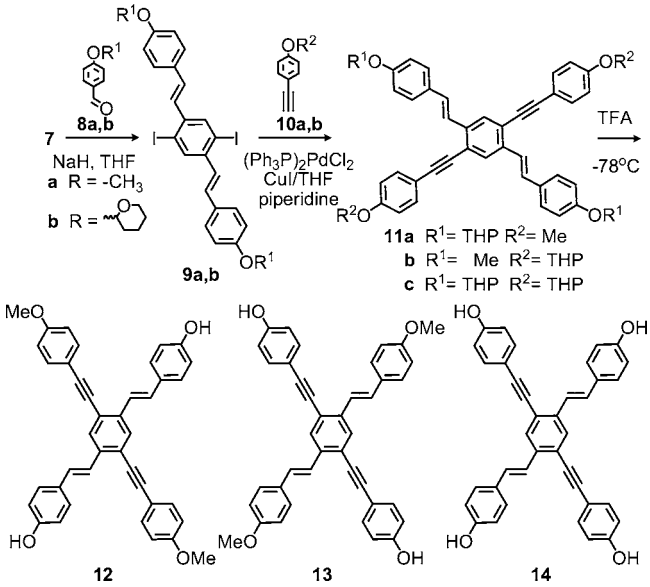

of the HOMO and LUMO should be more or less equally affected, resulting in only small net changes in the HOMO−LUMO gap.

A seductive strategy to develop responsive fluorophores would be to design molecular architectures possessing spatially separated FMOs. Here, electronic information becomes spatially encoded; recognition elements can be incorporated into the fluorophore such that analyte binding independently influences the FMOs. Therefore, analyte binding affects the energetic position of either HOMO or LUMO to a different degree, inducing a significant change in emission and absorption spectra. As a result, conjugated frameworks exhibiting FMO separation are intrinsically important as responsive materials.

Interest in materials possessing spatially separated FMOs has prompted the exploration of new two-dimensional, "X-shaped" conjugated materials,[1,2] including spiro compounds,[3] paracyclophanes,[4] swivel-type dimers,[5] bisoxazole-derived cruciforms,[6] tetraethynylethenes,[7] tetrasubstituted tolanes,[8] etc.[9] A subset of these compounds are constructed from two "perpendicular" π-conjugated linear arms connected through a central aromatic core; examples include tetrakis(arylethynyl)benzenes,[10,11] tetrakis(styryl)benzenes,[12,13] and tetrasubstituted thiophenes.[14]

This Account chronicles our investigation of specific two-dimensional conjugated architecture: 1,4-distyryl-2,5-bis(arylethynyl)benzenes (cruciforms, XFs).[15−26] While the term "cruciform" is often used to refer to other x-shaped materials, herein, the term cruciform refers exclusively to 1,4-distyryl-2,5-bis(arylethynyl)benzenes. We explore the design of XFs and examine their analyte-induced changes in fluorescence. XFs are composed of two linear π-conjugated segements, a perpendicular distyryl branch and an arylethynyl branch, connected via a central benzene core. Analysis of the electronic structure of XFs has revealed that donor and acceptor substitution results in compounds possessing FMOs spatially disjoint from one another; in these cases, the HOMO and LUMO localize on the "orthogonal" arms of XFs. How are the XFs different from Haley's tetraethynylbenzenes? Distyrylbenzenes are more electron-rich and have red-shifted absorption and emission compared with bis(phenylethylbenzene)s; their combination in the XFs generates a system where the inherent properties of the attached substituents are magnified when electron-donating substituents are attached to the distyrylbenzene axis and acceptor substituents are located on the arylethynyl axis. The large cation-induced changes in fluorescence displayed by XFs are observed to a far lesser extent in the tetrakis(arylethynyl)benzenes with identical substituent pattern. Fluorophores possessing spatially separated FMOs are uncommon in organic materials; however, this has significant consequences for the photophysics of XFs and has led to their use as building blocks in supramolecular assemblies,[23,24] components in molecular electronics,[15] and most notably as responsive cores in sensory schemes.[17−19,21,22,25,26]

Our examination of XFs highlights the importance of serendipity in the development of functional materials. The structural components and principles developed in diverse research areas serve as the inspiration for the construction of advanced materials. For example, Müllen's examination of the intramolecular [4 + 2]-cycloaddition reactions of phenylenevinylenes as well as Vollhardt's exploration of the cyclotrimerization of 1,2-diphenylethynes provided the synthetic underpinnings for the examination of a wealth of remarkable polycyclic aromatic hydrocarbons.[27] Similarly, our inspiration for XF architectures arose from examinations of cross-conjugated polymers. Our

efforts to probe the responsivity of XFs highlight the utility of FMO-separated materials as ratiometric cores in sensory applications.

The PPE Problem

The cruciform π-systems have grown out of a long-standing research interest in poly(*para*-phenylene ethynylene)s (PPEs, **1**), a class of conjugated polymers related to poly(phenylene vinylene)s (PPVs, **2**).[28] Unfortunately, PPEs do not share the balanced performance of PPVs in organic device applications; hole injection is a particular problem. Attempts to remedy this shortcoming by introducing vinyl groups into the main chain did not significantly improve performance; **3** resembles **1** much more than **2** with respect to its optical and solid state semiconducting properties.[29] In a second attempt to induce PPV character in PPEs, polymers of the type **4a**−**c**, incorporating styryl groups in the side chain, were studied.[30] In these polymers, the solution and solid state band gap shrinks from **4a** to **4c**. Hole injection is considerably facilitated, particularly in **4c**, which was explored in a photodiode-type application; **4c** is more electron-rich than PPV.[30] Cyclic voltammetry revealed that increasing donor strength in the distyrylbenzene arms (from **4a** to **4c**) exclusively affects the HOMO position. Only later would we come to understand the significance of this discovery: *these cross-conjugated architectures permit the spatial separation of FMOs*.

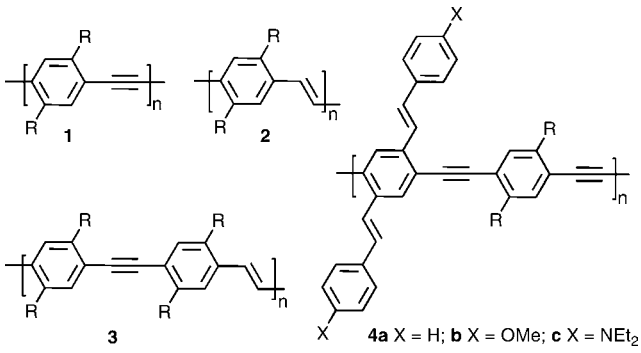

Synthesis of XFs

To better understand PPE−PPV hybrid polymers, we prepared a series of 1,4-distyryl-2,5-bisarylethynylbenzenes. The synthesis of XFs is simple. Starting from **5** (Scheme 1), bromination affords **6**, which is reacted with triethylphosphite to give **7** in an Arbuzov reaction. A subsequent Horner reaction with an aromatic aldehyde furnishes a diiodinated distyrylbenzene (DSB). Sonogashira alkynylation completes the synthetic sequence to give the cruciforms (XF).

Because both Horner and Sonogashira reactions are versatile, this synthetic sequence allows the construction of virtually any conceivable XF, as long as the desired aldehydes and alkynes are available. The introduction of hydroxyl functionalities necessitates protection because the Horner reaction must proceed under exclusion of water and oxygen. The synthesis of XFs with phenolic OH groups is shown in Scheme 2. Their synthesis is completed with the cleavage of the acetal protecting groups to furnish **12**−**14**. Other XFs containing phenothiazine, terpyridine, and phenylimidobisacetic acid units have also been prepared by this flexible two-step method. Figure 1 displays the distinct emission colors of a small selection of XFs as obtained by digital photography.

FIGURE 1. Emission of XFs **15**−**20** in dichloromethane under blacklight irradiation (λ_{max} = 365 nm).

Spectroscopic Properties of XFs

Initially, XFs were viewed as model compounds for PPEs **4a**−**4c**. However, we discovered that the photophysical properties of **15**−**20** could be tuned to a surprising extent by varying the substitution of the XF traverses. XFs **15**−**17** (Figure 2) display strong absorptions in hexanes at approximately 325 nm with a second feature appearing as a shoulder at slightly higher wavelengths (350−360 nm, Table 1). Upon introduction of donor (**18**) or donor−acceptor (**19** and **20**) substitution, we observe a charge transfer band at lower energy (~430 nm).

Even more dramatic trends are observed in the emission spectra of **15**−**20**. XF **15**, possessing no significant donor or acceptor substituents, displays a vibrant blue emission with a well-defined vibronic structure. Upon acceptor substitution, **16** and **17** retain the featured blue emission observed in the unsubstituted parent XF. Dibutylamino-substituted **18** displays a similar feature but red-shifted emission (λ_{max} em = 469 nm). Upon donor−acceptor substitution (**19** and **20**), the emission becomes increasingly red-shifted and the vibronic coupling disappears. XFs can be considered distyrylbenzene derivatives; **19** and **20** must possess significant charge transfer behavior. Also, greater positive solvatochromism is evident in the emission of the donor−acceptor XFs (Figure 3).

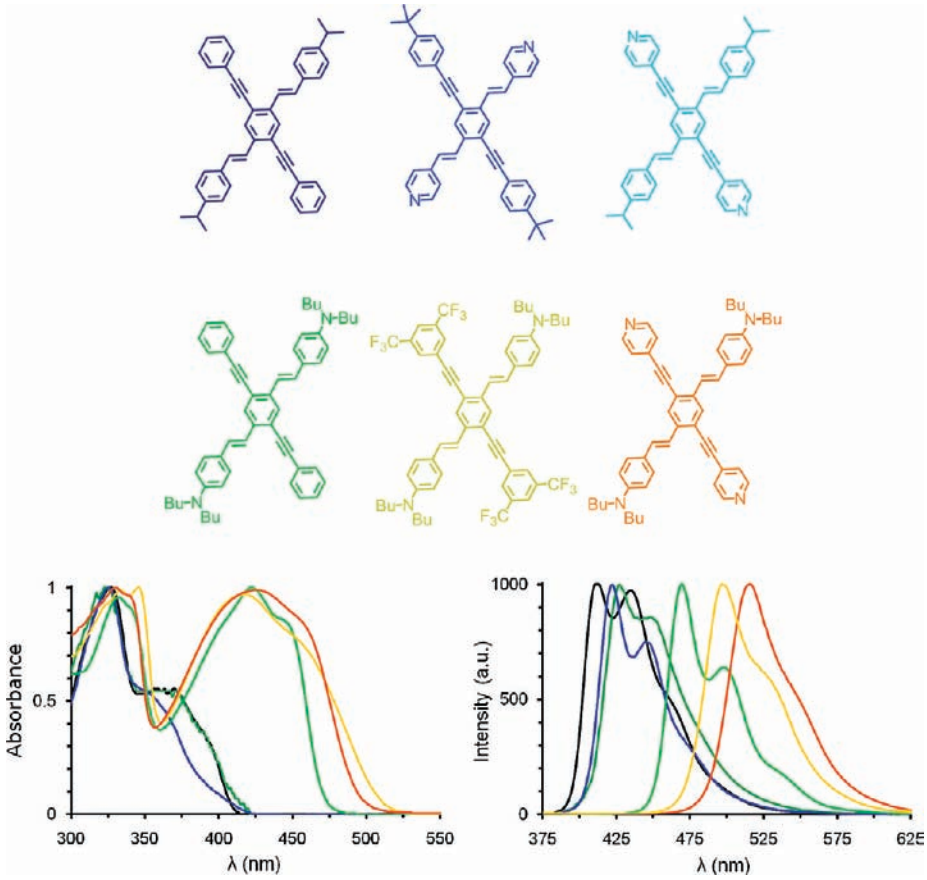

FIGURE 2. Normalized absorption (left) and emission (right) of XFs **15**−**20** in hexanes.

TABLE 1. Absorption and Emission Data of XFs **15**−**20** in Dichloromethane and Hexanes

XF	λ_{max} absorption in CH_2Cl_2 (nm)	λ_{max} emission in CH_2Cl_2 (nm)	λ_{max} absorption in hexanes (nm)	λ_{max} emission in hexanes (nm)	vibronic progression, cm^{-1}, (solvent)	quantum yield in $CHCl_3$	fluorescence lifetime, τ (ns),[a] in $CHCl_3$
15	396 sh	419	390 sh	409	1191 (CH_2Cl_2) 1302 (hex.)		
16	361 sh	444	353	422	1225 (hex.)	0.67	3.8
17	395 sh	456	390 sh	427	1097 (hex.)	0.70	4.0
18	436	519	447 sh	469	1242 (hex.)	0.31	1.7
19	472 sh	567	461 sh	516		0.09	4.3
20	472 sh	567	460 sh	496		0.11	4.3 4.3

[a] The lifetimes were monoexponential and fitted with a single decay function.

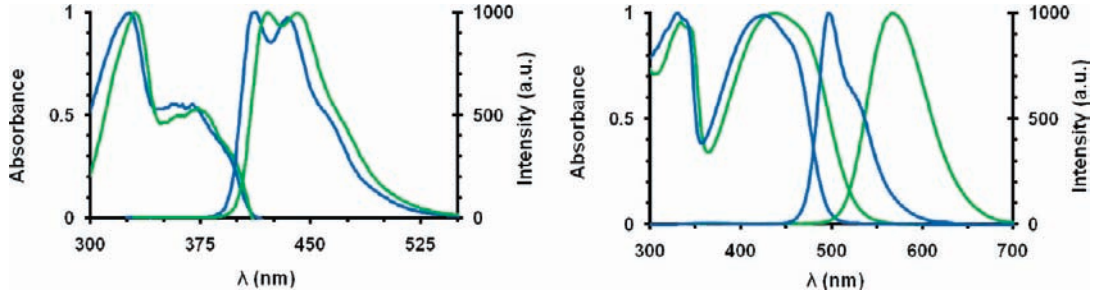

FIGURE 3. Normalized absorption and emission spectra of class C XF **15** (left) and class D XF **20** (right) in hexanes (blue trace) and dichloromethane (green trace).

Acceptor-substituted XFs **16** and **17** and donor-substituted **18** exhibit fluorescent quantum yields in halogenated solvents ranging from 0.70 (**17**) to 0.31 (**18**). Upon donor−acceptor substitution, the quantum yields of **19** and **20** drop

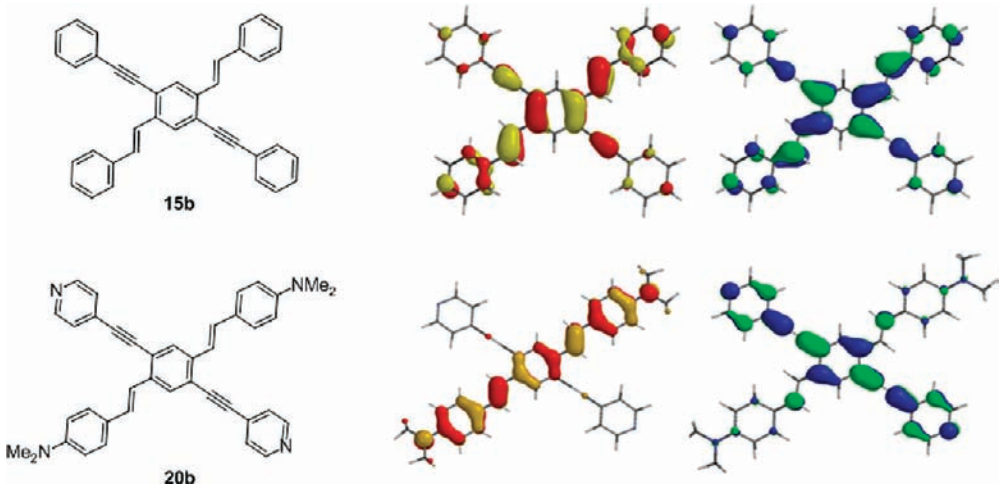

FIGURE 4. Frontier molecular orbitals of (top) **15b** (Spartan, B3LYP 6-31G**//6-31G**) showing (left) HOMO (−5.17 eV) and (right) LUMO (−2.00 eV) and (bottom) **20b** (Spartan, B3LYP 6-31G**//6-31G**) showing (left) HOMO (−4.63 eV) and (right) LUMO (−2.07 eV), which are now localized on the different branches of the molecule.

(0.09−0.11). Qualitatively, the quantum yield of these XFs appears inversely correlated with λ_{max} emission. This is not unexpected as compounds with smaller HOMO−LUMO gaps possess more accessible nonradiative mechanisms to relax to ground state. With the exception of **18** ($\tau = 1.7$ ns), the emissive lifetimes of the cruciforms are $\tau \approx 4$ ns, atypical for distyrylbenzene derivatives, which normally show shorter lifetimes of approximately $\tau \approx 1$ ns.

FMO Structure of XFs

Varying substitution of the XF framework results in differentiated spectroscopic properties. To rationalize their optical properties, we performed quantum chemical calculations on simplified analogues of XFs **15** and **20** (**15b** and **20b**). B3LYP 6-31G**//6-31G** calculations provide an understanding of ground state properties and HOMO−LUMO gaps when examining trends in a series of related compounds. In the unsubstituted parent XF **15b**, the HOMO and LUMO are evenly distributed over the π-system, with larger coefficients on the central benzene ring and smaller ones on the peripheral phenyl rings (Figure 4). This distribution is typical of π-conjugated hydrocarbons. Donor−acceptor substitution of the XF framework elicits a large change in the coefficient distribution of the FMOs. In the case of **20b**, possessing donor substituents on the distyryl axis of the XF and acceptor substituents on the arylethynyl axis of the XF, HOMO and LUMO show a spatially *disjoint* distribution. *The donor and acceptor substituents localize the FMOs on the respective arylethynyl and styryl branches*.

The ability of substitution to tune the FMO distribution, and as a result the optical properties, of XFs allows us to divide these chromophores into two subsets. *Class D* XFs show a *disjoint* FMO structure as a consequence of donor−acceptor substitution of the framework. On the other hand, cruciforms that are not significantly donor/acceptor substituted possess spatially superimposable FMOs; we propose to call these *class C* XFs in reference to their spatially *congruent* FMO arrangement. The distinction between class C and class D XFs is rigidly defined; however, the gradual transition between the two coincides with the appearance of a charge transfer band in the absorption spectra and a loss of vibronic features in the emission spectra.

Metallo- and Acidochromicity of XFs

Responsive fluorophores consist of a binding element capable of interacting with the target analyte affixed to a conjugated core, which affords an optical response. If recognition elements are suitably integrated into FMO-separated fluorophores, analyte binding can independently affect the energy level of either the HOMO or LUMO, resulting in a large observable spectroscopic change. XFs possessing Lewis-basic nitrogens incorporated into the π-electron system provide an opportunity to probe the sensory responses of XFs when exposed to model analytes such as trifluoroacetic acid (TFA) or $Zn(OTf)_2$.

XFs Exhibiting a Two-Stage Fluorescence Response: A Case Study. We exposed **20** to both TFA and Zn^{2+}. Upon addition of increasing equivalents of Zn^{2+} ions to **20** in chloroform, a rare two-stage fluorescence response is observed: the emission color changes from orange to blue and then to green (Figure 5). A similar response is observed upon addition of TFA to **20**.[31]

A spectrophotometric titration of **20** with $Zn(OTf)_2$ in dichloromethane was performed (Figure 6). The absorption

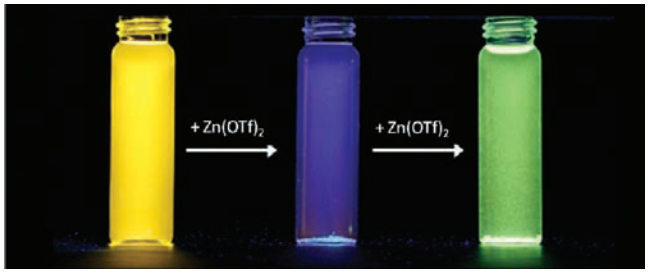

FIGURE 5. Emission of **20** in chloroform (left vial, orange emission), upon addition of a small amount of $Zn(OTf)_2$ (center vial, blue emission), and upon addition of a large excess of $Zn(OTf)_2$ (right vial, green emission).

of **20** consists of a high-energy band at 335 nm and a charge transfer peak centered at 440 nm. Upon addition of Zn^{2+}, the charge transfer feature disappears accompanied by a small shift (335 → 350 nm) in the high-energy band. In the emission, upon addition of a small quantity of $Zn(OTf)_2$, a large blue shift (570 → 420 nm) occurs; subsequent addition of Zn^{2+} results in a bathochromic shift (420 → 530 nm).

This two-stage response can be rationalized by examining the sensory response of **17** and **18**; these XFs are bona fide models of **20** possessing either pyridyl or dibutylamino substituents. In the case of **18**, only a hypsochromic shift (527 → 430 nm) is observed upon addition of Zn^{2+} (Figure 7). Consideration of the FMO arrangement in **18** offers an explanation; B3LYP 6-31G**//6-31G** calculations suggest that the HOMO is localized primarily on the distyryl axis of the XF. Binding of Zn^{2+} to the aniline nitrogens of **18** lowers the HOMO energy while leaving the LUMO largely unperturbed. As a result, a blue shift in emission is observed (Figure 9a). XF **17** contains exclusively the pyridyl binding functionalities on the arylethynyl axis. Upon reac-

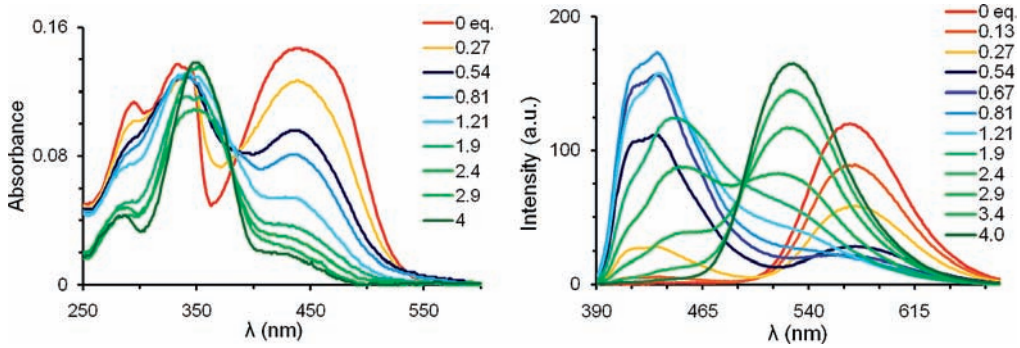

FIGURE 6. Absorption (left) and emission (right) of **20** in dichloromethane upon exposure to increasing equivalents of zinc triflate.

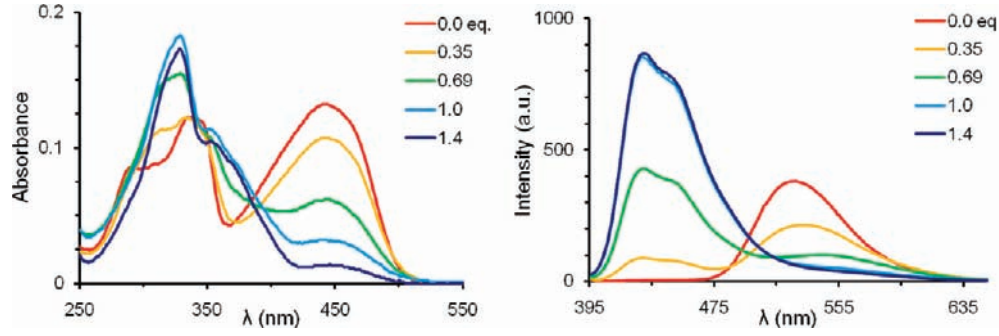

FIGURE 7. Absorption (left) and emission (right) of **18** in dichloromethane upon exposure to increasing equivalents of zinc triflate.

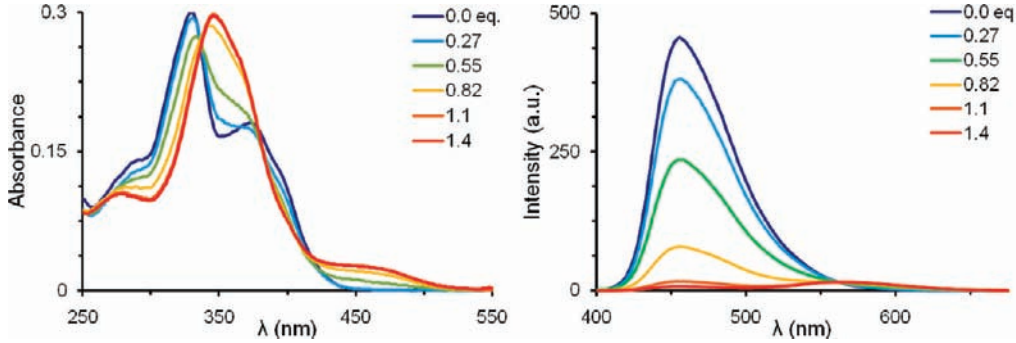

FIGURE 8. Absorption (left) and emission (right) of **17** in dichloromethane upon exposure to increasing equivalents of zinc triflate.

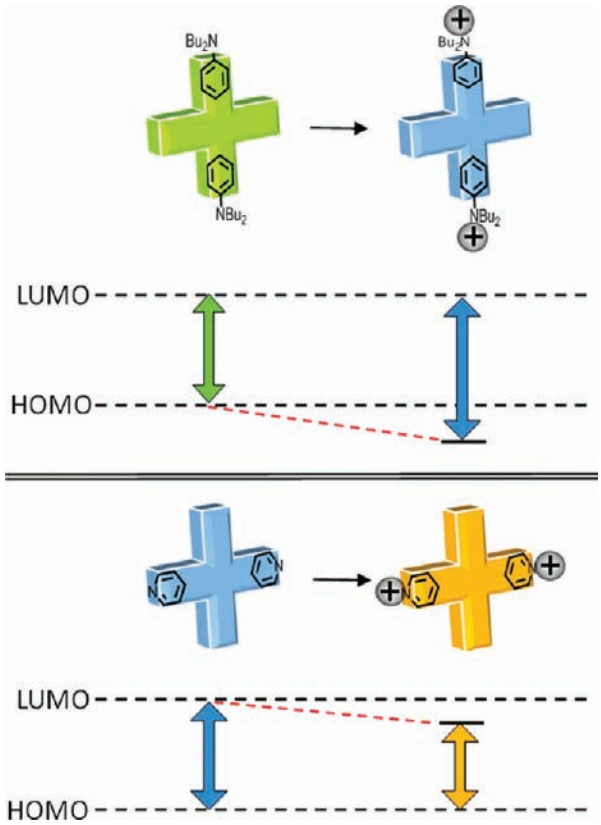

FIGURE 9. Schematic representation of the effect of metalation or protonation upon the FMOs and emission of XFs **18** (top) and **17** (bottom).

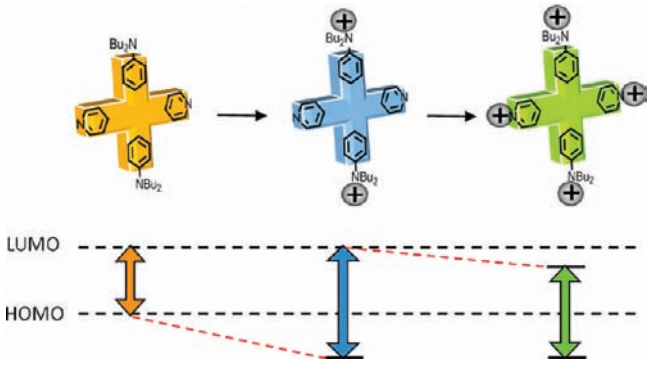

FIGURE 10. Schematic representation of the effect of metalation or protonation upon the FMOs and emission of XF **20**.

tion with zinc triflate, a red shift in emission (457 → 564 nm) is observed (Figure 8). Zinc coordination of the pyridyl nitrogens lowers the LUMO energy of **17**, which lies along the arylethynyl axis of the XF scaffold, while the HOMO is unaffected (Figure 9b).

The two-stage fluorescence response of **20** can be understood in light of models **17** and **18** (Figure 10). Upon addition of Zn^{2+} to **20**, coordination first occurs at the anilines, lowering the HOMO energy while leaving the LUMO unaffected, generating the initial blue shift. Subsequent addition of Zn^{2+} coordinates the pyridyl nitrogens of **20**; this interaction lowers the LUMO energy, causing the second bathochromic shift.

Comparing Metals and Acid: Elucidating the Nature of Analyte Interaction. The responses observed upon exposure of XFs to metal ions raises questions as to the locus and stoichiometry of analyte interaction. In the case of alkylamino-functionalized XFs, it is of interest to determine whether the metal cation coordinates to the aniline nitrogen or to the electron-rich π-face of the aromatic ring.[32] In addition, it is important to determine whether the sensory response results from the coordination of one or both available nitrogens on an XF branch. In the case of protons, both the stoichiometry and locus of binding are known: an excess of TFA added to **16**−**20** will protonate all available nitrogens. Comparing the spectroscopic responses observed for Zn^{2+} with those found for TFA will reveal whether a similar mode of analyte interaction with the XF exists. The absorption, emission, fluorescence quantum yield, and fluorescence lifetimes of **16**−**20** were measured upon addition of excess zinc triflate and trifluoroacetic acid (Table 2 and Figure 11). In all cases, *similar changes are observed in the spectroscopic properties of* **16**−**20** *upon addition of either TFA or* Zn^{2+}. This suggests that the metal cations are coordinating through the Lewis-basic nitrogens and not via the arene rings.

We conducted ^{1}H NMR studies of representative XFs (Figure 12). Similar shifts in the proton NMR spectra occur upon addition of either Zn^{2+} or TFA, offering further confirmation that both analytes interact via the Lewis-basic nitrogen. Upon analyte addition, we observe only one set of sharp signals

TABLE 2. Spectroscopic Properties of XFs **16**−**20** upon Addition of Excess Trifluoroacetic Acid or Zinc Trifluoromethanesulfonate

	excess TFA				excess $Zn(OTf)_2$			
XF	λ_{max} absorption in CH_2Cl_2 (nm)	λ_{max} emission in CH_2Cl_2 (nm)	quantum yield in $CHCl_3$	fluorescence lifetime, τ (ns), in $CHCl_3$[a]	λ_{max} absorption in CH_2Cl_2 (nm)	λ_{max} emission in CH_2Cl_2 (nm)	quantum yield in $CHCl_3$	fluorescence lifetime, τ (ns), in $CHCl_3$[a]
16	339	532	0.06	7.2	339	543	0.18	6.9
17	350	555		3.5	356	580	0.31	3.9
18	330	425	0.44	2.8	328	429	0.62	3.0
19	337	430	0.68	3.0	336	429	0.84	2.8
20	343	509	0.06	2.0	340	518	0.11	2.1

[a] The lifetimes were monoexponential and fitted with a single decay function.

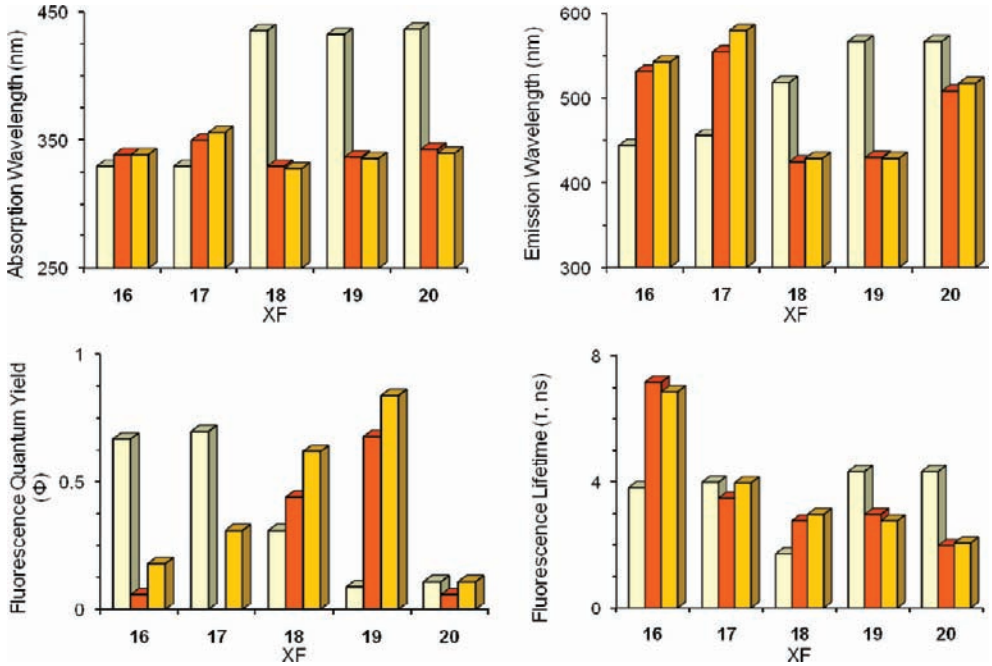

FIGURE 11. Comparison of the observed photophysical responses of XFs **16**−**20** (beige bar) toward TFA (dark orange bar) and $Zn(OTf)_2$ (light orange bar).

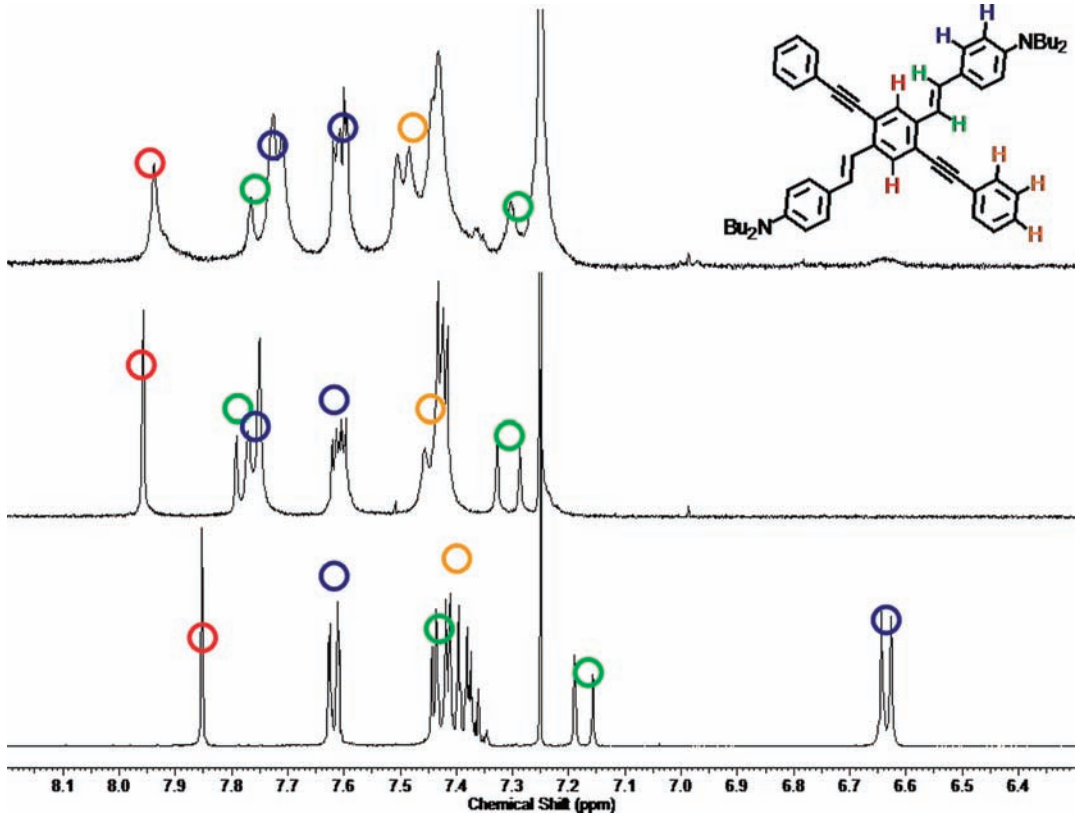

FIGURE 12. ^1H NMR spectra of **18** ($CDCl_3$): top, after addition of an excess of zinc triflate; middle, after addtion of an excess of trifluoroacetic acid; bottom, no additives. All spectra were taken at 400 MHz.

consistent with a symmetrical, doubly bound species. In the event that only the monoprotonated/metalated species was formed, we would expect to observe either broadened signals or a more complex series of signals consistent with an asymmetric product. Apparently, metal cations bind to these XFs via alkylamino nitrogens, and the observed spectral response results from the coordination of all available Lewis-basic nitrogens.

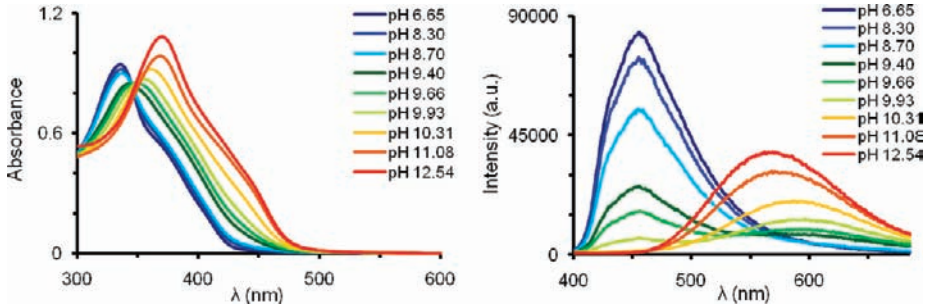

FIGURE 13. Spectrophotometric titration of **14** with sodium hydroxide in 2:1 MeOH/H_2O.

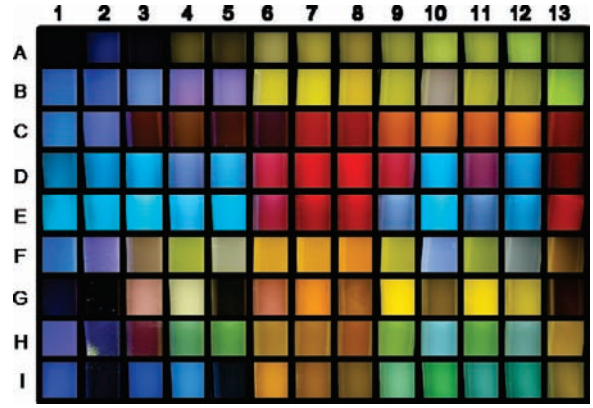

FIGURE 14. Photograph of solutions (λ_{max} ex = 365 nm) of **14** upon addition of amines 2−13 (left to right)—(1) **14**, (2) histamine (6.9), (3) imidazole (6.9), (4) morpholine (8.3), (5) piperazine (9.8), (6) putrescine (9.9), (7) 1,3-diaminopropane (10.5), (8) ethylenediamine (10.7), (9) piperidine (10.8), (10) triethylamine (10.8), (11) diethylamine (11.0), (12) diisopropylamine (11.1), and (13) 1,8-diazabicyclo[5.4.0]undec-7-ene (DBU, ~12) [numbers in parentheses are the pK_a values of the corresponding ammonium ions in water]—in different solvents (top to bottom)—(A) 90:10 water/methanol, (B) methanol, (C) acetonitrile, (D) DMF, (E) DMSO, (F) THF, (G) dichloromethane, (H) diethyl ether, and (I) toluene.

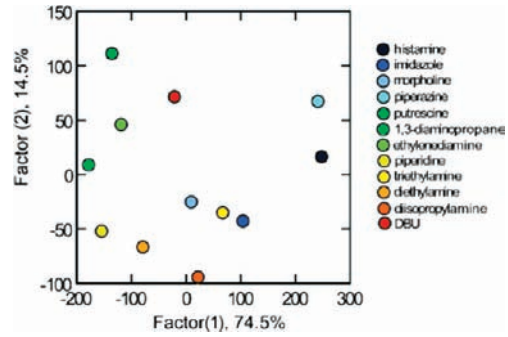

FIGURE 15. LDA results demonstrating the identification of 12 amines using **14** in nine different solvents. The plot was extracted from the RGB values measured from the photographs of **14** with amines in nine solvents (Figure 14).

Response of Hydroxy XFs toward Amines

The detection and quantification of aliphatic amines is important in environmental science, the pharmaceutical industry, and dye manufacturing. Amines pollute soil, landfills, manufacturing sites, and aqueous environs. Biogenic amines (histamine, putrescine) form by enzymatic decarboxylation of amino acids and indicate food spoilage for fish products.[33] Their detection has been achieved by a variety of methods.[34−37] To further examine the potential utility of XFs as sensory cores, we examined **12**−**14**, possessing strategically placed phenol functionalities.[25,26]

XFs **12**−**14** display blue emission (λ_{max} 450−475) and quantum yields in the range of 0.16−0.37. Titration of **12**−**14** with KOH demonstrated that in the case of **12**, deprotonation results in a new band at 416 nm in the absorption spectra and a shift in the emission spectra (460 → 600 nm). Deprotonation of **13** led to quenching. Upon deprotonation of **14**, an isosbestic point is visible at 346 nm and a new absorption maximum develops at 370 nm. When pH is changed from pH 7 to 10, we observe an even more red-shifted (588 nm) emission band of lower intensity. Upon further increase of the pH, the fluorescence intensity of **14** increases again and the emission maximum shifts to 565 nm (Figure 13).

Solutions of **12**−**14** were prepared in nine different solvents, and representative amines were added. While some shifts in emission were observed in the case of **12**, exposure of amines to **14** resulted in solutions with emission colors ranging from blue to red traversing yellow and green, *spanning the full visible spectral range* (Figure 14). From these observations, we concluded that the difference in pK_a between hydroxy-XFs and amines is sufficient to produce a solvent-separated ion pair in the excited state.[38] In the ground state, the observed ΔpK_a results in the formation of hydrogen-bonded complexes. Utilizing the Kamlet−Taft method,[39] we determined that the increase of solvent polarity and basicity causes the bathochromic shift of the emission, while the acidity of the solvent works in the opposite direction. While it is not clear why each amine displays different shifts in emission, it is dependent upon the structure of the amine and the chemical environment.

The results obtained for **14** exposed to amines in varied solvents was analyzed by linear discriminant analysis (LDA) using matrices derived by simply extracting the RGB values in

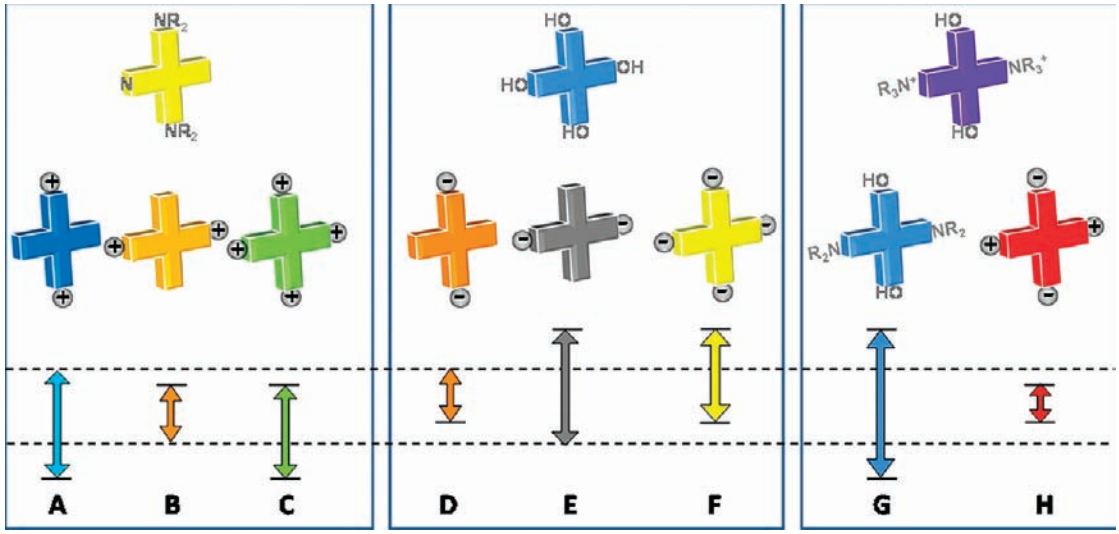

FIGURE 16. Schematic representation of the potential sensory responses elicited by the binding of cationic or anionic species or both to symmetrically functionalized XFs. Eight different binding scenarios are conceivable resulting in five unique fluorescence responses. The dotted lines indicate the position of the frontier molecular orbitals of the parent XF, while the solid lines indicate the changes to the FMOs upon binding of a cation or an anion to the XF.

Figure 14 (Figure 15). Surprisingly, all 12 amines can be discerned. These experiments imply that a "chemical nose" need not involve large numbers of unique sensors; rather, variable responsivity can be achieved by employing one sensor molecule in different chemical environments. We note that this phenomenon has important implications for the future design of simple yet powerful differential sensor arrays.

Conclusions

Moving beyond one-dimensional molecular wire-type fluorophores to two-dimensional X-shaped materials provides access to conjugated architectures with unexpected and exciting properties. XFs represent such novel conjugated architectures. Donor−acceptor substitution results in materials that have been employed as building blocks in supramolecular coordination assemblies[23,24] and used as switches in molecular electronics;[15] however, their FMO architecture makes XFs attractive for sensing applications as demonstrated in the case of amines.

FMO-separated XFs provide an opportunity to develop responsive materials; by spatially separating HOMO and LUMO on a conjugated framework, analytes can independently address these FMOs, translating electronic into spatial information. Large changes in optical properties result upon analyte recognition. Figure 16 schematically represents the possible responses for pair wise symmetrically substituted XFs. If both positively and negatively charged species are allowed to interact with functionalized XFs, *eight different electronic responses* (A−H) *exhibiting unique emission colors will result*. In case A, coordination of an electron-deficient analyte (i.e., a proton or metal cation) with the HOMO branch of an XF lowers the energy of the HOMO, yielding a blue-shifted emission. In case B, binding to the LUMO-containing axis of the XF elicits a red-shifted emission. These effects are reversed in cases D and E where an anion or an electron-releasing species interacts with the XF; here, the position of the HOMO or the LUMO energies are raised, leading to a red shift in case D and an expected quenching in case E. If all four termini are bound by an analyte (cases C and F), only slight net shifts should be visible. In principle, either a blue or a red shift could be observed; however, in the case of C (**20**), we observe a slight net blue shift, while in case F we observe a significant red shift.

Thus far, we have successfully constructed and explored cases **A**−**F**. Future efforts will examine further functionalization of the XF core to achieve the interesting and challenging cases **G** and **H**. In the case of **G**, addition of an electron-releasing analyte to the HOMO branch and an electron-deficient species to the LUMO branch, the position of the LUMO is raised while that of the HOMO is lowered; a dramatic blue shift is expected. In case **H**, we predict the opposite effect, where LUMO is lowered and HOMO is raised; emission in the red or near-IR will result. These final examples will fully unveil the potential responses of the XFs. Additional responsive diversity can be introduced with XFs if the distyryl and arylethynyl branches are asymmetrically substituted, highlighting the importance of new conjugated architectures.

We acknowledge J. Wilson, J. Tolosa, S. Brombosz, K. Solntsev, M. Hauck, J. Schönhaber, R. Phillips, and Y. Wang and

helpful discussions with Profs. Tolbert, Fahrni, Müller, Weck, and Perry. We thank the National Science Foundation (Grants DMR 0138948 and NSF-CHE 0750275) and Georgia Tech for financial support. A.J.Z. acknowledges the Center for Organic Photonics and Electronics at Georgia Tech for a graduate research fellowship. P.L.M. acknowledges a FACES (Facilitating Academic Careers In Engineering and Science) at Tech for a graduate fellowship.

BIOGRAPHICAL INFORMATION

Anthony J. Zucchero was born in 1982 in St. Louis, Missouri. In 2004, he received a B.S. in chemistry from the University of the South. He is currently a graduate student at working in the Bunz group.

Psaras McGrier was born in 1982 in Abbeville, South Carolina. He obtained his B.S. in chemistry in 2004 from the University of South Carolina—Aiken. In 2005, Psaras joined the Bunz group at Georgia Tech.

Uwe Bunz (1963) studied Chemistry at the LMU Munich where he received his Ph.D. in 1990. A postdoctoral position (1991−1992) with Vollhardt at UC Berkeley was followed by his Habilitation in Mainz under the auspices of Müllen. From 1997 to 2003, he taught at the University of South Carolina (Columibia). Since 2003, he has held a position as Full Professor at the School of Chemistry and Biochemistry at the Georgia Institute of Technology. His hobbies are cooking/baking, swimming (not competitive), and long board surfing (poorly). He is interested in alkynes.

FOOTNOTES

*To whom correspondence should be addressed. Fax: 404-385-1795. Tel: 404-510-2443. E-mail: uwe.bunz@chemistry.gatech.edu.

REFERENCES

1 Opsitnick, E.; Lee, D. Two-dimensional electronic conjugation: Statics and dynamics at structural domains beyond molecular wires. *Chem.—Eur. J.* **2007**, *13*, 7040–7049.

2 Galbrecht, F.; Bünnagel, T.; Bilge, A.; Scherf, U.; Farrell, T. Cruciform-Conjugated Oligomers. In *Functional Organic Materials - Syntheses, Strategies, and Applications*; Müller, T. J. J., Bunz, U. H. F., Eds.; Wiley-VCH: Weinheim, Germany, 2007; pp 83−118.

3 (a) Saragi, T. P. I.; Spehr, T.; Siebert, A.; Fuhrmann-Lieker, T.; Salbeck, J. Spiro compounds for organic optoelectronics. *Chem. Rev.* **2007**, *107*, 1011–1065. (b) Shirota, Y.; Kageyama, H. Charge carrier transporting molecular materials and their applications in devices. *Chem. Rev.* **2007**, *107*, 953–1010.

4 (a) Bartholomew, G. P.; Bazan, G. C. Bichromophoric paracyclophanes: Models for interchromophore delocalization. *Acc. Chem. Res.* **2001**, *34*, 30–39. (b) Bartholomew, G. P.; Rumi, M.; Pond, S. J. K.; Perry, J. W.; Tretiak, S.; Bazan, G. C. Two-photon absorption in three-dimensional chromophores based on [2.2]-paracyclophane. *J. Am. Chem. Soc.* **2004**, *126*, 11529–11542.

5 (a) Zen, A.; Pingel, P.; Jaiser, F.; Neher, D.; Grenzer, J.; Zhuang, W.; Rabe, J. P.; Bilge, A.; Galbrecht, F.; Nehls, B. S.; Farrell, T.; Scherf, U.; Abellon, R. D.; Grozema, F. C.; Siebbeles, L. D. A. Organic field-effect transistors utilizing solution-deposited oligothiophene-based swivel cruciforms. *Chem. Mater.* **2007**, *19*, 1267–1276. (b) Bilge, A.; Zen, A.; Forster, M.; Li, H.; Galbrecht, F.; Nehls, B. S.; Farrell, T.; Neher, D.; Scherf, U. Swivel-cruciform oligothiophene dimers. *J. Mater. Chem.* **2006**, *16*, 3177–3182.

6 (a) Klare, J. E.; Tulevski, G. S.; Sugo, K.; de Picciotto, A.; White, K. A.; Nuckolls, C. Cruciform π-systems for molecular electronics applications. *J. Am. Chem. Soc.* **2003**, *125*, 6030–6031. (b) Klare, J. E.; Tulevski, G. S.; Nuckolls, C. Chemical reactions with upright monolayers of cruciform π-systems. *Langmuir* **2004**, *20*, 10068–10072. (c) Florio, G. M.; Klare, J. E.; Pasamba, M. O.; Werblowsky, T. L.; Hyers, M.; Berne, B. J.; Hybertsen, M. S.; Nuckolls, C.; Flynn, G. W. Frustrated Ostwald ripening in self-assembled monolayers of cruciform π-systems. *Langmuir* **2006**, *22*, 10003–10008.

7 (a) Nielsen, M. B.; Diederich, F. Conjugated oligoenynes based on the diethynylethene unit. *Chem. Rev.* **2005**, *105*, 1837–1867. (b) Kivala, M.; Diederich, F. Acetylene-derived strong organic acceptors for planar and nonplanar push-pull chromophores. *Acc. Chem. Res.* **2009**, *42*, 235–248.

8 Tolosa, J.; Díez-Barra, E.; Sánchez-Verdú, P.; Rodríguez-López, J. Unsymmetrically substituted four-armed tolanes: New multichromophoric molecules. *Tetrahedron Lett.* **2006**, *47*, 4647–4651.

9 (a) Zhao, C.-H.; Wakamiya, A.; Inukai, Y.; Yamaguchi, S. Highly emissive organic solids containing 2,5-diboryl-1,4-phenylene unit. *J. Am. Chem. Soc.* **2006**, *128*, 15934–15935. (b) Blaszczyk, A.; Fischer, M.; von Hanisch, C.; Mayor, M. The synthesis of molecular rods with a transversal push-pull system. *Eur. J. Org. Chem.* **2007**, *16*, 2630–2642.

10 (a) Marsden, J. A.; Miller, J. J.; Shirtcliff, L. D.; Haley, M. M. Structure-property relationships of donor/acceptor-functionalized tetrakis(phenylethynyl)benzenes and bis(dehydrobenzoannuleno)benzenes. *J. Am. Chem. Soc.* **2005**, *127*, 2464–2476. (b) Spitler, E. L.; Shirtcliff, L. D.; Haley, M. M. Dynamic proton-induced two-stage emission switching in donor-functionalized bis(dehydrobenzo[n]annuleno)benzenes and 1,2,4,5-tetrakis(phenylethynyl)benzene. *J. Org. Chem.* **2007**, *72*, 86–96. (c) Slepkov, A. D.; Hegmann, F. A.; Tykwinski, R. R.; Kamada, K.; Ohta, K.; Marsden, J. A.; Spitler, E. L.; Miller, J. J.; Haley, M. H. Two-photon absorption in two-dimensional conjugated quadrupolar chromophores. *Opt. Lett.* **2006**, *31*, 3315–3317. (d) Spitler, E. L.; Haley, M. M. Dynamic proton-induced two-stage emission switching in donor-functionalized bis(dehydrobenzo[n]annuleno)benzenes and 1,2,4,5-tetrakis(phenylethynyl)benzene. *Tetrahedron* **2008**, *64*, 11469–11474.

11 Moore, A. M.; Dameron, A. A.; Mantooth, B. A.; Smith, R. K.; Fuchs, D. J.; Ciszek, J. W.; Maya, F.; Yao, Y.; Tour, J. M.; Weiss, P. S. Molecular engineering and measurements to test hypothesized mechanisms in single molecule conductance switching. *J. Am. Chem. Soc.* **2006**, *128*, 1959–1967.

12 (a) Niazimbetova, Z. I.; Christian, H. Y.; Bhandari, Y. J.; Beyer, F. L.; Galvin, M. E. Design and development of novel 2-D oligomers for electroactive device application. *J. Phys. Chem. B* **2004**, *108*, 8673–8681. (b) Christian-Pandya, H. K.; Niazimbetova, Z. I.; Beyer, F. L.; Galvin, M. E. Role of symmetry and charge delocalization in two-dimensional conjugated molecules for optoelectronic applications. *Chem. Mater.* **2007**, *19*, 993–1001.

13 (a) Kang, H.; Evmenenko, G.; Dutta, P.; Clays, K.; Song, K.; Marks, T. J. X-shaped electro-optic chromophore with remarkably blue-shifted optical absorption. synthesis, characterization, linear/nonlinear optical properties, self-assembly, and thin film microstructural characteristics. *J. Am. Chem. Soc.* **2006**, *128*, 6194–6205. (b) Hu, K.; Zhu, P. W.; Yu, Y.; Facchetti, A.; Marks, T. J. Self-assembled electrooptic thin films with remarkably blue-shifted optical absorption based on an X-shaped chromophore. *J. Am. Chem. Soc.* **2004**, *126*, 15974–15975.

14 (a) Hsu, H.-F.; Kuo, C.-H.; Chen, C.-F.; Lin, Y.-H.; Huang, L.-Y.; Chen, C.-H.; Cheng, K.-C.; Chen, H.-H. Synthesis and mesomorphic properties of multiynylthiophenes: 2,3,4,5-tetrakis(4-alkoxyphenylethynyl)thiophenes and 2,3,5-tris(4-alkoxyphenylethynyl)thiophenes. *Chem. Mater.* **2004**, *16*, 2379–2385. (b) Sun, X. B.; Zhou, Y. H.; Wu, W. C.; Liu, Y. Q.; Tian, W. J.; Yu, G.; Qiu, W. F.; Chen, S. Y.; Zhu, D. B. X-shaped oligothiophenes as a new class of electron donors for bulk-heterojunction solar cells. *J. Phys. Chem. B* **2006**, *110*, 7702–7707.

15 Grunder, S.; Huber, R.; Horhoiu, V.; González, M. T.; Schönenberger, C.; Calame, M.; Mayor, M. New cruciform structures: Toward coordination induced single molecule switches. *J. Org. Chem.* **2007**, *72*, 8337–8344.

16 Wilson, J. N.; Hardcastle, K. I.; Josowicz, M.; Bunz, U. H. F. Synthesis and electronic properties of bis-styryl substituted trimeric aryleneethynylenes. Comparison of cruciforms with *iso*-cruciforms. *Tetrahedron* **2004**, *60*, 7157–7167.

17 Wilson, J. N.; Bunz, U. H. F. Switching of intermolecular charge-transfer in cruciforms: metal ion sensing. *J. Am. Chem. Soc.* **2005**, *127*, 4124–4125.

18 Zucchero, A. J.; Wilson, J. N.; Bunz, U. H. F. Cruciforms as functional fluorophores: Response to protons and selected metal ions. *J. Am. Chem. Soc.* **2006**, *128*, 11872–11881.

19 Tolosa, J.; Zucchero, A. J.; Bunz, U. H. F. Water-soluble cruciforms: Response to protons and selected metal ions. *J. Am. Chem. Soc.* **2008**, *130*, 6498–6506.

20 Wilson, J. N.; Smith, M. D.; Enkelmann, V.; Bunz, U. H. F. Cruciform π-systems: Effect of aggregation on emission. *Chem. Commun.* **2004**, 1700–1701.

21 Brombosz, S. M.; Zucchero, A. J.; Phillips, R. L.; Vazquez, D.; Wilson, A.; Bunz, U. H. F. Terpyridine-based cruciform-Zn^{2+} complexes as anion-responsive fluorophores. *Org. Lett.* **2007**, *22*, 4519–4522.

22 Hauck, M.; Schönhaber, J.; Zucchero, A. J.; Hardcastle, K. I.; Müller, T. J. J.; Bunz, U. H. F. Phenothiazine cruciforms: Synthesis and metallochromic properties. *J. Org. Chem.* **2007**, *72*, 6714–6725.

23 Gerhardt, W. W.; Zucchero, A. J.; Wilson, J. N.; South, C. R.; Bunz, U. H. F.; Weck, M. Supramolecular cruciforms. *Chem. Commun.* **2006**, 2141–2143.

24 Gerhardt, W. W.; Zucchero, A. J.; South, C. R.; Bunz, U. H. F.; Weck, M. Controlling polymer properties through dynamic metal-ligand interactions: supramolecular cruciforms made easy. *Chem.—Eur. J.* **2007**, *13*, 4467–4474.

25 McGrier, P. L.; Solntsev, K. M.; Schönhaber, J.; Brombosz, S. M.; Tolbert, L. M.; Bunz, U. H. H. Hydroxy-cruciforms. *Chem. Commun.* **2007**, 2127–2129.

26 McGrier, P. L.; Solntsev, K. M.; Miao, S.; Tolbert, L. M.; Miranda, O. R.; Rotello, V. M.; Bunz, U. H. F. Hydroxycruciforms: Amine-responsive fluorophores. *Chem.—Eur. J.* **2008**, *14*, 4503–4510.

27 (a) Vollhardt, K. P. C. Transition-metal-catalyzed acetylene cyclizations in organic synthesis. *Acc. Chem. Res.* **1977**, *10*, 1–8. (b) Berresheim, A. J.; Müller, M.; Müllen, K. Polyphenylene nanostructures. *Chem. Rev.* **1999**, *99*, 1747–1785. (c) Watson, M. D.; Fechtenkötter, A.; Müllen, K. Big is beautiful—"Aromaticity" revisited from the viewpoint of macromolecular and supramolecular benzene chemistry. *Chem. Rev.* **2001**, *101*, 1267–1300.

28 (a) Bunz, U. H. F. Poly(aryleneethynylene)s: Syntheses, properties, structures, and applications. *Chem. Rev.* **2000**, *100*, 1605–1644. (b) Bunz, U. H. F. Poly(aryleneethynylene)s. *Macromol. Rapid Commun.* **2009**, *30*, 772–805.

29 Tekin, E.; Egbe, D. A. M.; Kranenburg, J. M.; Ulbricht, C.; Rathgeber, S.; Birckner, E.; Rehmann, N.; Meerholz, K.; Schubert, U. S. Effect of side chain length variation on the optical properties of PPE—PPV hybrid polymers. *Chem. Mater.* **2008**, *20*, 2727–2735.

30 (a) Wilson, J. N.; Windscheif, P. M.; Evans, U.; Myrick, M. L.; Bunz, U. H. F. Band gap engineering of poly(*p*-phenyleneethynylene)s: Cross-conjugated PPE—PPV hybrids. *Macromolecules* **2002**, *35*, 8681–8683. (b) Wilson, J. N.; Josowicz, M.; Wang, Y.; Bunz, U. H. F. Cruciform π-systems: Hybrid phenylene-ethynylene/phenylene-vinylene oligomers. *Chem. Commun.* **2003**, 2962–2963.

31 Fahrni, C. J.; Yang, L. C.; VanDerveer, D. G. Tuning the photoinduced electron-transfer thermodynamics in 1,3,5-triaryl-2-pyrazoline fluorophores: X-ray structures, photophysical characterization, computational analysis, and in vivo evaluation. *J. Am. Chem. Soc.* **2003**, *125*, 3799–3812.

32 Hirsch, K. A.; Wilson, S. R.; Moore, J. S. Association of dicyanodiphenylacetylenes with silver(I) salts in solution and solid state: Electrospray ionization mass spectrometry samples aggregates at subsaturated concentrations. *J. Am. Chem. Soc.* **1997**, *119*, 10401–10412.

33 (a) Guy, P. A.; Gremaud, E.; Richoz, J.; Turesky, R. J. Quantitative analysis of mutagenic heterocyclic aromatic amines in cooked meat using liquid chromatography-atmospheric pressure chemical ionisation tandem mass spectrometry. *J. Chromatogr. A.* **2000**, *883*, 89–102. (b) Morrow, J. D.; Margolies, G. R.; Rowland, J.; Roberts, L. J. Evidence that histamine is the causative toxin of scombroid-fish poisoning. *N. Engl. J. Med.* **1991**, *324*, 716–720.

34 (a) Greene, N. T.; Shimizu, K. D. Colorimetric molecularly imprinted polymer sensor array using dye displacement. *J. Am. Chem. Soc.* **2005**, *127*, 5695–5700. (b) Mertz, E.; Zimmerman, S. C. Cross-linked dendrimer hosts containing reporter groups for amine guests. *J. Am. Chem. Soc.* **2003**, *125*, 3424–3425. (c) Maynor, M. S.; Nelson, T. L.; O'Sullivan, C.; Lavigne, J. J. A food freshness sensor using the multistate response from analyte-induced aggregation of a cross-reactive poly(thiophene). *Org. Lett.* **2007**, *9*, 3217–3220.

35 Yeh, C.-Y.; Lin, S.-J.; Hwang, D.-F. Biogenic amines, histamine and label of dressed fried fish meat products in Taiwan. *Food Control* **2004**, *17*, 423–428.

36 (a) Rakow, N. A.; Sen, A.; Janzen, M. C.; Ponder, J. B.; Suslick, K. S. Molecular recognition and discrimination of amines with a colorimetric array. *Angew. Chem., Int. Ed.* **2005**, *44*, 4528–4532. (b) Suslick, K. S.; Rakow, N. A.; Sen, A. Colorimetric sensor arrays for molecular recognition. *Tetrahedron* **2004**, *60*, 11133–11138. (c) Rakow, N. A.; Suslick, K. S. A colorimetric sensor array for odour visualization. *Nature* **2000**, *406*, 710–713. (d) Wright, A. T.; Anslyn, E. V. Differential receptor arrays and assays for solution-based molecular recognition. *Chem. Soc. Rev.* **2006**, *35*, 14–28. (e) Lavigne, J. J.; Anslyn, E. V. Sensing a paradigm shift in the field of molecular recognition: From selective to differential receptors. *Angew. Chem., Int. Ed.* **2001**, *40*, 3118–3130.

37 Ruiz-Capillas, C.; Moral, A. Production of biogenic amines and their potential use as quality control indices for hake (*Merluccius merluccius*, L.) stored in ice. *J. Food Sci.* **2001**, *66*, 1030–1032.

38 Zaitsev, N. K.; Demyashkevich, A. B.; Kuzmin, M. G. Effect of the acid-base properties of the reagents on proton phototransfer reactions in the solid-phase. *High Energy Chem.* **1980**, *14*, 116–120.

39 Kamlet, M. J.; Abboud, J.-L. M.; Abraham, M. H.; Taft, R. W. Linear solvent relationships. 23. A comprehensive collection of the solvatochromic parameters, π^*, α, and β, and some methods for simplifying the generalized solvatochromic equation. *J. Org. Chem.* **1983**, *48*, 2877–2887.